ACS APPLIED MATERIALS & INTERFACES

www.acsami.org

Research Article

Piezoelectricity Enhancement of Nanogenerators Based on PDMS and $ZnSnO_3$ Nanowires through Microstructuration

Ana Rovisco, Andreia dos Santos, Tobias Cramer, Jorge Martins, Rita Branquinho, Hugo Águas, Beatrice Fraboni, Elvira Fortunato, Rodrigo Martins, Rui Igreja,* and Pedro Barquinha*

Cite This: *ACS Appl. Mater. Interfaces* 2020, 12, 18421−18430

Read Online

ACCESS | Metrics & More | Article Recommendations | Supporting Information

ABSTRACT: The current trend for smart, self-sustainable, and multifunctional technology demands for the development of energy harvesters based on widely available and environmentally friendly materials. In this context, $ZnSnO_3$ nanostructures show promising potential because of their high polarization, which can be explored in piezoelectric devices. Nevertheless, a pure phase of $ZnSnO_3$ is hard to achieve because of its metastability, and obtaining it in the form of nanowires is even more challenging. Although some groups have already reported the mixing of $ZnSnO_3$ nanostructures with polydimethylsiloxane (PDMS) to produce a nanogenerator, the resultant polymeric film is usually flat and does not take advantage of an enhanced piezoelectric contribution achieved through its microstructuration. Herein, a microstructured composite of nanowires synthesized by a seed-layer free hydrothermal route mixed with PDMS ($ZnSnO_3$@PDMS) is proposed to produce nanogenerators. PFM measurements show a clear enhancement of d_{33} for single $ZnSnO_3$ versus ZnO nanowires (23 ± 4 pm/V vs 9 ± 2 pm/V). The microstructuration introduced herein results in an enhancement of the piezoelectric effect of the $ZnSnO_3$ nanowires, enabling nanogenerators with an output voltage, current, and instantaneous power density of 120 V, 13 μA, and 230 μW·cm^{-2}, respectively. Even using an active area smaller than 1 cm^2, the performance of this nanogenerator enables lighting up multiple LEDs and other small electronic devices, thus proving great potential for wearables and portable electronics.

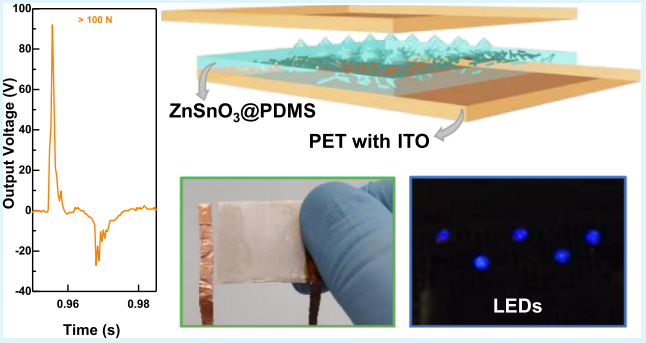

KEYWORDS: *piezoelectricity, $ZnSnO_3$, nanowires, PDMS, micro-structuration, nanogenerator*

INTRODUCTION

Nowadays, there is an increasing demand for smart, self-sustainable, and multifunctional technology to enable concepts such as internet-of-things, relying on low-cost, and compact devices. The vision is to expand smart-functionality with embedded electronics, sensors, and connectivity to an ever-increasing number of objects. The development of self-powered sensors that harvest the ambient environmental energy will be the key toward these systems and is mandatory to be in line with the preservation of the global environment and sustained economic growth.[1]

One great renewable electricity source is vibration energy harvesting, which has been explored essentially from electromagnetic, electrostatic, and piezoelectric transduction.[2,3] Electromagnetic energy harvesters are the least reported ones, with an output voltage that is poorer when compared with the other two types, despite being the most suitable for low-frequency stimuli.[4] Piezoelectric nanogenerators (PENG) are the most used transducers for mechanical vibrations, human motion, stream flow, and acoustic noise.[5] This type of energy harvester provides higher output voltages and is more efficient at high frequencies.[1,4,6] Finally, electrostatic transduction is typically based on the triboelectric effect that causes an electric potential difference when a periodic gap or mismatch is induced by friction between two contacted surfaces with opposite triboelectric polarities.[7] In a triboelectric nanogenerator (TENG), this physical contact creates electrostatic charges, driving the electrons to flow back and forth between back-coated electrodes, meaning this phenomenon is more efficient for a low-frequency range.[1,2] Therefore, PENGs and TENGs have a high potential for different applications such as sustainable energy sources, biomedical systems, and smart sensors.[8,9]

Several materials have been used for piezoelectric energy harvesters, the most common being Pb(Zr, Ti)O_3 (PZT), P(VDF-TrFE), PTFE, ZnO, $ZnSnO_3$, $BaTiO_3$, and GaN.[2,10−14] Although PZT is the one with the highest

Received: December 3, 2019
Accepted: March 20, 2020
Published: March 20, 2020

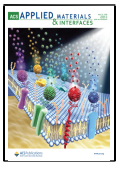

https://dx.doi.org/10.1021/acsami.9b21636
ACS Appl. Mater. Interfaces 2020, 12, 18421−18430

piezoelectric constant, its conductivity is low and it is environmentally harmful.[5] When looking for sustainable options it is important to avoid toxic and nonrecyclable materials but also those which are scarce. Within these premises, Zn-based metal oxides such as ZnO and $ZnSnO_3$ are some of the most promising materials. ZnO has been widely used because of its easy synthesis and coupling of piezoelectric and semiconductor properties.[1,15−19] $ZnSnO_3$ appears to be an even better candidate for energy harvesting applications, having a higher polarization (≈59 $\mu C/cm^2$) along the *c*-axis.[20] Moreover, the advantages of zinc tin oxide (ZTO) are numerous. Not only are both zinc and tin abundant and recyclable, but ZTO is also a ternary oxide, its properties can be tuned by adjusting the cationic ratio, boosting its multifunctionality. Depending on the synthesis method, different morphologies can be obtained and $ZnSnO_3$ can crystallize in two different structures, rhombohedral and orthorhombic, undergoing a phase transformation into Zn_2SnO_4 at high temperatures (>700 °C).[21−25] However, the presence of two cations in ZTO makes the synthesis of a pure single phase very hard to achieve. Several reports about the application of $ZnSnO_3$ micro- and nanostructures in PENGs and TENGs were published in the last few years. $ZnSnO_3$ nanocubes have been the most reported structure with piezoelectric and piezoresistive effects for applications in energy harvesting and sensitive human motion sensors.[1,5,26−33] More recently, in 2017 Guo et al. reported piezo-nanogenerators using flat films of polydimethylsiloxane (PDMS) mixed with $ZnSnO_3$ nanoplates, produced by a hydrothermal method, showing the difficulty to obtain a single and pure phase of this material by solution processing.[5] Concerning $ZnSnO_3$ micro/nanowires, there are only a few reports of generators making use of vapor phase synthesis methods. In 2012 and 2013, Wu et al. reported nanogenerators of $ZnSnO_3$ microbelts, produced by thermal evaporation at 900 °C, generating a power output around 11 $\mu W \cdot cm^{-3}$.[26,28,34] Furthermore, these $ZnSnO_3$-based nanogenerators are generally based in flat films of a mixture of PDMS or other polymers and oxide nano- or microstructures[5,28,31−33,35−37] or simply use PDMS to encapsulate such structures,[26,34] therefore not taking advantage of the microstructuration of the polymeric film to increase the efficiency in the transduction of a force into an electrical output.[12,38−44]

In a previous work, a seed-layer free hydrothermal route at 200 °C was optimized to produce well-controlled $ZnSnO_3$ nanowires.[24] The microstructuration of the PDMS film by a laser engraving technique was also studied and optimized by our group to produce piezoresistive sensors, where several architectures were developed.[45−47] Here, we combine, for the first time, these two recent techniques to microstructure a robust composite of nanowires mixed with PDMS ($ZnSnO_3$@PDMS) into microcones, thus improving the efficiency of the force delivery to the nanowires and greatly increasing their piezoelectric signal. Because of this effect the device presents a high potential for energy harvesting applications.

EXPERIMENTAL SECTION

$ZnSnO_3$ Nanowires' Synthesis. The $ZnSnO_3$ nanowires were produced by a hydrothermal synthesis in a conventional oven using $SnCl_4 \cdot 5H_2O$ from Riedel-de Haën (0.01 M), $ZnCl_2$ from Merck (0.02 M), and NaOH from Sigma-Aldrich (0.24 M) as precursors and H_2O and ethylenediamine from Sigma-Aldrich in a volume proportion of 7.5:7.5 mL as solvents, at 200 °C for 24 h, based on our previous works.[24,48] The resultant precipitate of nanowires' syntheses was centrifuged at 6000 rpm and washed several times with deionized water and isopropyl alcohol, alternately. The nanostructures were finally dried at 60 °C, in vacuum, for 2 h.

Nanogenerator Fabrication. Four acrylic molds were used, combining aligned or misaligned microcone cavities with measured gaps between cones of 0 or <100 μm. These acrylic molds were produced on a previous work.[45] A laser engraving machine (VLS3.50, 50 W, Universal Laser System, USA) with a CO_2 laser beam, a lens' focus focal length of 2.0 in., a focal spot of 127 μm in diameter, a power of 25 W, and a speed of 0.1524 $m \cdot s^{-1}$ was used to engrave acrylic plates (Dagol, 5 mm thick, squares of 5 cm × 5 cm) with designs based in the repetition of symmetrical crosses (size of 100 μm) distributed over an area of 2 cm × 2 cm in an aligned or misaligned way and spaced by a theoretical gap between cones of 150 or 300 μm. The final functional area of the devices is 4 cm^2.

The $ZnSnO_3$ nanowires were mixed with PDMS with a weight ratio of 20 wt %. Then, the curing agent was added to the previous mixture in a 1:10 w/w ratio of curing agent to elastomer. The mixture was then spin-coated onto each mold at 250 rpm for 90 s, and degassed before curing the $ZnSnO_3$@PDMS composite in an oven at 85 °C. After 30 min of curing, a commercial polyethylene terephthalate substrate covered with indium tin oxide (PET/ITO) substrate (Kintec Company) was placed on top of composite films, which were left in the oven until completing the curing. This PET/ITO substrate played the role of the bottom electrode in the device. After peeling off the composite bounded to PET/ITO, another PET/ITO substrate was placed on top of the microstructured face to work as a top electrode. Both substrates were tightly secured to each other by using kapton tape (DuPont). For an easier connection to external equipment, copper tape (3M) was used as an extension of each electrode of the nanogenerator.

$ZnSnO_3$ Nanowire, Composite, and Nanogenerator Characterization. The structural characterization of the produced $ZnSnO_3$ nanowires and $ZnSnO_3$@PDMS composite was done using a PANalytical's X'Pert PRO MRD diffractometer with Cu Kα radiation. The X-ray diffraction (XRD) data were acquired in the 10−90° 2θ range with a step size of 0.033°. The morphology and element analysis [scanning electron microscopy/energy-dispersive X-ray (SEM/EDS)] were performed with a Carl Zeiss AURIGA CrossBeam (FIB-SEM) workstation. To investigate the properties of the composite, cured films of the $ZnSnO_3$@PDMS composite without microstructuration were spin-coated with the same parameters as previously mentioned and aluminum electrodes (100 nm) were evaporated on their surface. As a comparison, the same was performed for only PDMS. A constant force of approximately 10 N was applied by a home-made machine (Figure S1) with a linear motor at a frequency of 2 pushes per second to all composites and devices. The contact area for these tests was 0.3 cm^2. Besides, the home-made machine, in order to test the devices with different forces, a pen was used to apply human force between 12 and >100 N in an area of 0.7 cm^2. The output voltage was collected by a digital oscilloscope (Tektronix TDS 2001C, 10 MΩ input impedance), while the current output signals were acquired using a Keysight B1500A system. The force applied in the produced devices was estimated using a commercial force sensing resistor from Interlink Electronics (ref. SEN05003). The capacitance of PDMS and the $ZnSnO_3$@PDMS composite was measured using a Keysight B1500A system. In order to compare the results of $ZnSnO_3$ nanowires with well-known structures, the same characterization was performed for synthesized ZnO nanowires based on ref 49 (Supporting Information, Figure S2). Piezoelectric force microscopy was performed with a NX10 Park-Systems setup using Micromash NSC36CrAu probes. Sparse nanowires on ITO substrates were detected in a noncontact mode. Piezoresponse measurements were subsequently performed by contacting a single point on the nanowire surface and applying an AC signal of 1 to 4 V to the tip at 17 kHz.

https://dx.doi.org/10.1021/acsami.9b21636
ACS Appl. Mater. Interfaces 2020, 12, 18421−18430

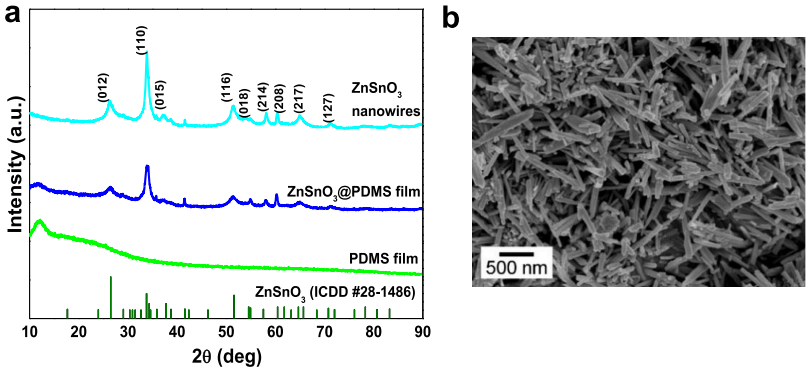

Figure 1. (a) XRD patterns of PDMS, $ZnSnO_3$@PDMS film, and $ZnSnO_3$ nanowires before mixing with PDMS. The identification was following ICDD card #28-1486 as explained in ref 24. (b) SEM image of $ZnSnO_3$ nanowires.

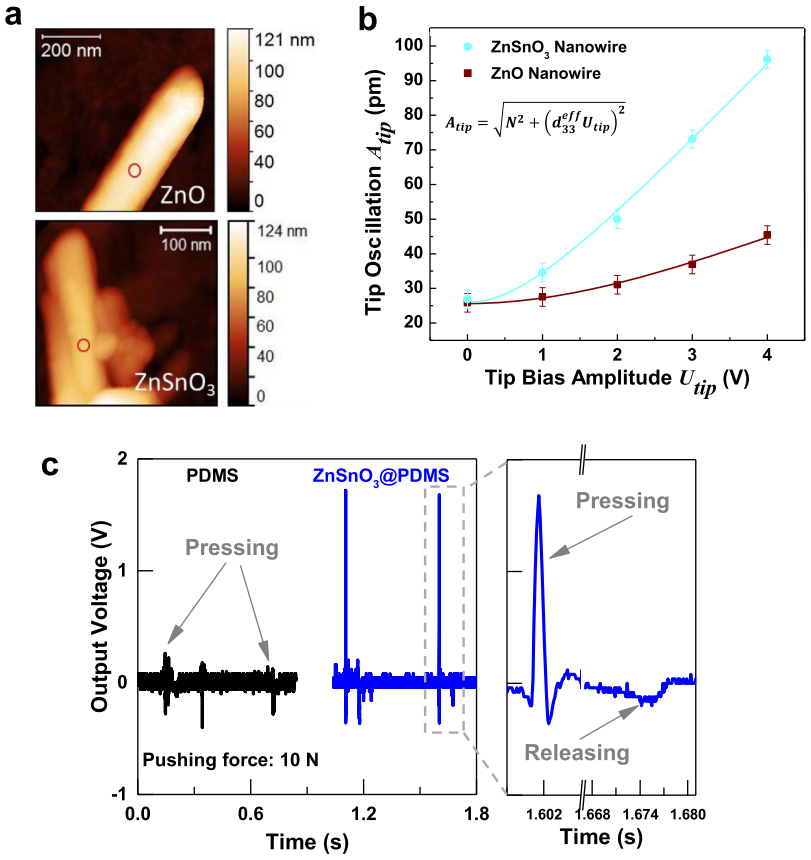

Figure 2. Atomic force microscopy to characterize the piezoresponse of individual ZnO and $ZnSnO_3$ nanowires: (a) nanowire topographies of ZnO and $ZnSnO_3$ obtained in noncontact mode (the red spot indicates the area that was contacted in piezoresponse measurements); (b) contact mode tip oscillation as a function of tip-bias ac-voltage to extract the effective piezocoefficient d_{33}. (c) Piezoelectric response of $ZnSnO_3$@PDMS and only PDMS for a pushing force of 10 N. The inset shows the output of $ZnSnO_3$@PDMS with a greater detail, highlighting the peaks corresponding to the pressing and releasing of the composite.

RESULTS AND DISCUSSION

Characterization of $ZnSnO_3$ Nanowires and $ZnSnO_3$@PDMS Films. Figure 1 shows the XRD patterns and morphology of $ZnSnO_3$ nanowires. These structures have an average length of 600 nm and diameter of 65 nm. Concerning the crystalline structure identification, although the #28-1486 card was deleted from the ICDD database, this card fits well with a $ZnSnO_3$ orthorhombic phase. In ref 24, this identification was proven. Moreover, this card has been also widely reported as a $ZnSnO_3$ orthorhombic phase, emphasizing the identification.[30,50−53]

Electromechanical properties of individual and unpolarized nanowires were characterized by atomic force microscopy (Figure 2a,b). Piezoresponse curves were obtained by contacting a single spot on the nanowire surface and are shown in Figure 2b for ZnO and $ZnSnO_3$. For ZnO, the response is slightly above the noise level and leads to an effective piezoelectric constant of d_{33} = 9 ± 2 pm/V, in agreement with the values reported for ZnO nanostructures.[54] The $ZnSnO_3$ structures instead yield almost three times stronger responses leading to d_{33} = 23 ± 4 pm/V. This value compares fairly well with what has been reported in the

https://dx.doi.org/10.1021/acsami.9b21636
ACS Appl. Mater. Interfaces 2020, 12, 18421−18430

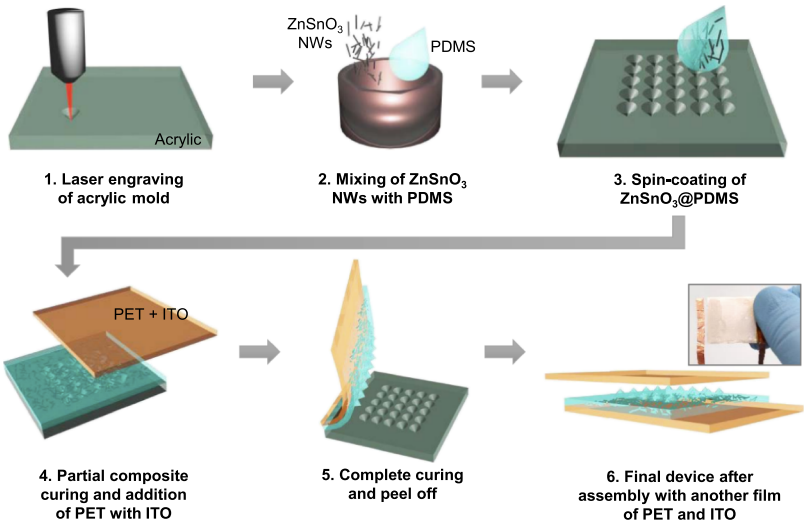

Figure 3. Fabrication steps of a microstructured nanogenerator. The inset is a photograph of one nanogenerator.

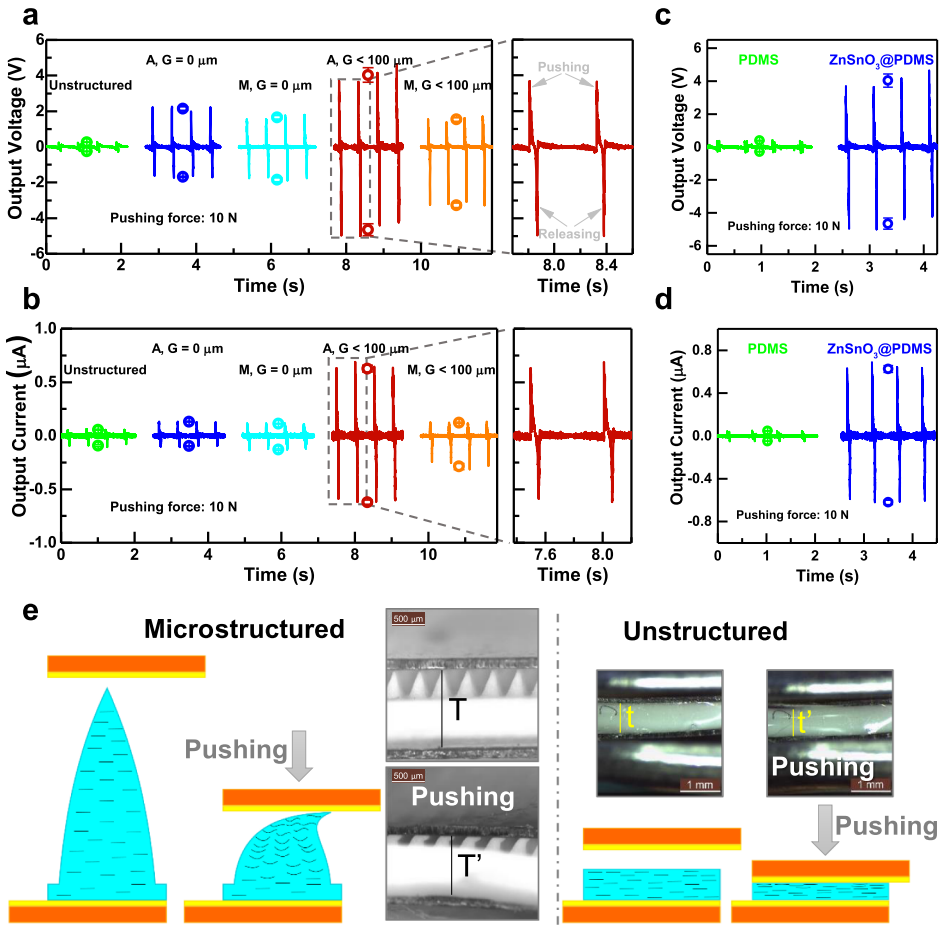

Figure 4. Output (a) voltage and (b) current generated from the $ZnSnO_3$@PDMS device with different configurations: unstructured films, microstructured films with aligned or misaligned microcones with a gap between cones of 0 or <100 μm. Output (c) voltage and (d) current generated from only PDMS and $ZnSnO_3$@PDMS microstructured films devices with aligned microcones with a gap between cones of <100 μm. The circles represent average values with standard deviations (of 4−6 measurements) for positive and negative peaks. Abbreviations: A—aligned, M—misaligned, G—gap. (e) Proposed schematics of force deformation for a microstructured and unstructured device and photographs showing the cross section of the devices before and after pushing force. Note that the schemes are not at scale. T (1.2 mm) and T' (940 μm) and t (782 μm) and t' (724 μm) are the thicknesses of the microstructured/unstructured $ZnSnO_3$@PDMS films before and after pushing, respectively.

literature for one-dimensional (1D) nanostructures produced by a hydrothermal synthesis, as assumed by Ghasemian et al. and presented in Table S1.[55] In fact, the obtained d_{33} (23 ± 4 pm/V) is surpassed only by the well-known $BaTiO_3$ (31.1 pm/V) and $LiNbO_3$ (25 pm/V) which contain critical raw materials, highlighting the interest in $ZnSnO_3$ for piezoelectric

https://dx.doi.org/10.1021/acsami.9b21636
ACS Appl. Mater. Interfaces 2020, 12, 18421−18430

applications. Additionally, electrostatic force microscopy (see Figure S3) shows that the relaxed nanowires do not exhibit static surface charges which could impact on their electromechanical response. Thus, the findings demonstrate the piezoelectric properties of the individual nanowires.

In order to investigate the piezoelectric effect of the $ZnSnO_3$@PDMS composite and to compare it with a film of only PDMS, electrodes of aluminum were directly evaporated on both surfaces of these samples to avoid any air gaps between the films and the electrodes, thus preventing any triboelectric effect. Subsequently, the samples were subjected to a mechanical stimulus of 10 N. In Figure 2c, it is clear that PDMS has barely any voltage generation upon pushing, which is expectable given that PDMS is not a piezoelectric material. The small signal recorded is coming from the interference with the electrodes.

The piezoelectric coefficient (d_{33}) value of a material can be determined according to: $d_{33} = Q/F$, where Q is the electric charge and F is the force. Knowing that the charge can be obtained by: $Q = C \times V$, where C is the capacitance and V is the voltage, the expression for d_{33} becomes: $d_{33} = C \times V/F$.[56] To clarify that the voltage output differences for PDMS and $ZnSnO_3$@PDMS are not coming from different capacitance values, the capacitance of these materials was measured, achieving values of 7.3 and 10 pF, respectively, for samples with the same area (≈3 cm^2). Given that the capacitance of the $ZnSnO_3$@PDMS composite is higher than PDMS, and assuming similar d_{33} coefficient for both, the $ZnSnO_3$@PDMS composite output voltage should be smaller. However, as shown in Figure 2c, the output voltage for the composite is much higher than for PDMS, suggesting a larger d_{33} of $ZnSnO_3$@PDMS, which was determined as ≈2 pm/V. Therefore, the $ZnSnO_3$@PDMS composite presents an evident piezoelectric response which must be attributed to the $ZnSnO_3$ nanowires.

Optimization of the Devices' Architecture. Herein, two different nanogenerator architectures (an unstructured and a microstructured one) were explored to study the influence of the microcones of the $ZnSnO_3$@PDMS composite in the devices' performance. The fabrication process of the microstructured nanogenerators is illustrated in Figure 3, where the microcavities with the shape of inverted cones are engraved by laser in acrylic plates. Four different engraving designs were explored to obtain aligned or misaligned microcones with different gaps between cones (0 or <100 μm). The microstructured films with the dimensions of the microcones can be seen in Figure S4. As it is further explored in ref 45, the measured gaps between cones (0 or <100 μm) are smaller than the gaps between cones that are used in the design imported to the laser engraving machine (150 or 300 μm, respectively) because of the melting of the mold's material (acrylic) during the engraving of the cavities. After molds' engraving, the $ZnSnO_3$@PDMS composite is spin-coated on the molds, being the composite capped by PET/ITO substrates in both sides, to work as bottom and top electrodes. A photograph of a final device is shown in the inset of Figure 3. For the unstructured $ZnSnO_3$@PDMS device, instead of spin-coating the composite over molds, the composite is spin-coated directly over the bottom electrode, and the top electrode is placed over the free surface of the composite after a partial curing.

For a better comparison between the devices and to achieve more reproducible results, a home-made machine (Figure S1 and Supporting Information Video S1) was used with a pushing force of 10 N and a pushing area of 0.3 cm^2. Despite the limitation on the force intensity applied through this machine, it allows to correctly compare all the samples, guaranteeing that the output differences between them are due to their different compositions, instead of different forces in the case of manual stimulation. Unless otherwise stated, this machine was used to mechanically stimulate all the samples analyzed in this work. Figure 4a,b shows the output voltage and current of devices with the different configurations previously described, highlighting the reproducibility of the output for each repeated stimulus. The unstructured device has a smaller piezoelectric output than the one presented in Figure 2c (for which an evaporated electrode was employed) because of an irregular contact between the top PET/ITO substrate and the $ZnSnO_3$@PDMS composite. Nevertheless, the results evidence that the presence of microstructuration gives rise to a higher output when compared to unstructured devices. Even though the microstructuration of the films reduces the effective contact area between the composite and the electrode, it is thought that it concentrates the compressive forces into the cones (Supporting Information Video S2), and so upon their compression and deformation, the nanowires dispersed in the microstructures undergo a greater compression/bending. This translates into more charges being induced at the electrode, resulting in a greater piezoelectric signal. The compressive forces do not actuate so effectively upon the nanowires in unstructured devices, which is illustrated in Figure 4e and Supporting Information Video S3. Therefore, in the unstructured nanogenerators the nanowires suffer less mechanical deformation resulting in lower charge induction and consequently in smaller outputs, even though their contact area with the electrode is larger.

The microstructuration of the composite also induces the presence of air gaps between the basis of the cones and the top electrode, which contributes to the induction of charges by a triboelectric effect. This is verified in Figure S5, where a microstructured device of only PDMS shows a higher output voltage and current than an unstructured one. To investigate the relevance of the triboelectric effect contribution to the performance of the $ZnSnO_3$@PDMS composite nanogenerators, microstructured devices of only PDMS and $ZnSnO_3$@PDMS with aligned microcones with a gap between cones of <100 μm were tested under the same conditions as previously described, with the results shown in Figure 4c,d. If the triboelectric effect was the main effect contributing to the performance of the nanogenerators, then $ZnSnO_3$@PDMS would have an output similar to that of only PDMS, where its output can only come from the triboelectricity generated between PDMS and ITO. However, the PDMS device shows a peak-to-peak voltage (0.7 V) and current (95 nA) output much smaller than the respective values for the $ZnSnO_3$@PDMS nanogenerator with the same configuration (8.7 V and 1.25 μA). Therefore, the output results for the $ZnSnO_3$@PDMS nanogenerator point toward an enhanced piezoelectric effect resultant from the structuration of the composite into microcones, which is the dominant effect dictating the performance of this type of nanogenerators. Based on these findings, a proposed charge generation and displacement mechanism for both the piezoelectric and triboelectric effects in microstructured devices is illustrated in Figure S6.

Regarding the different designs explored herein, devices with aligned cones present a slightly higher voltage than devices with misaligned cones, while for a current output the alignment

https://dx.doi.org/10.1021/acsami.9b21636
ACS Appl. Mater. Interfaces 2020, 12, 18421−18430

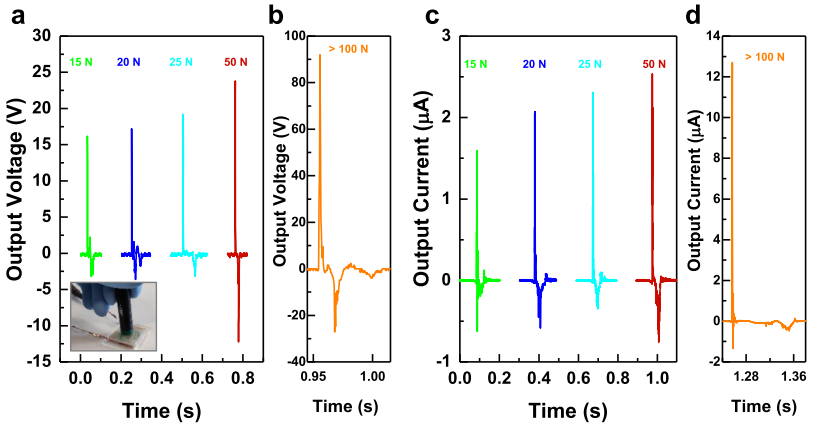

Figure 5. Output (a,b) voltage and (c,d) current of the nanogenerator with the optimized configuration, generated by applying a human force from 15 to 50 N and over 100 N using a pen (inset) to deliver the stimulus.

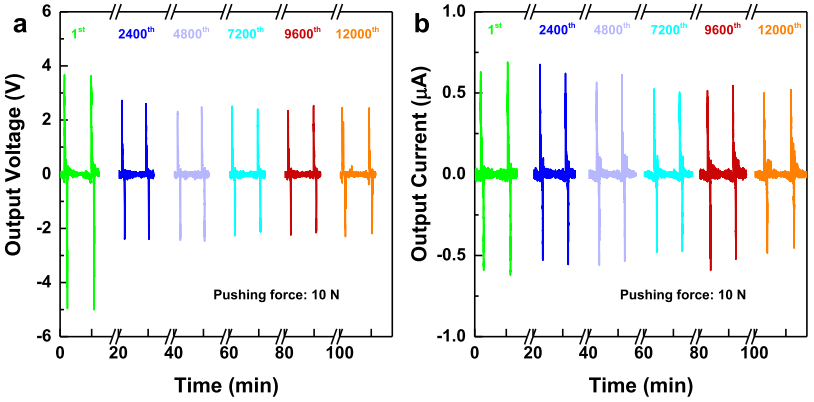

Figure 6. Output (a) voltage and (b) current generated from the nanogenerator with the optimized configuration for 12,000 cycles (100 min).

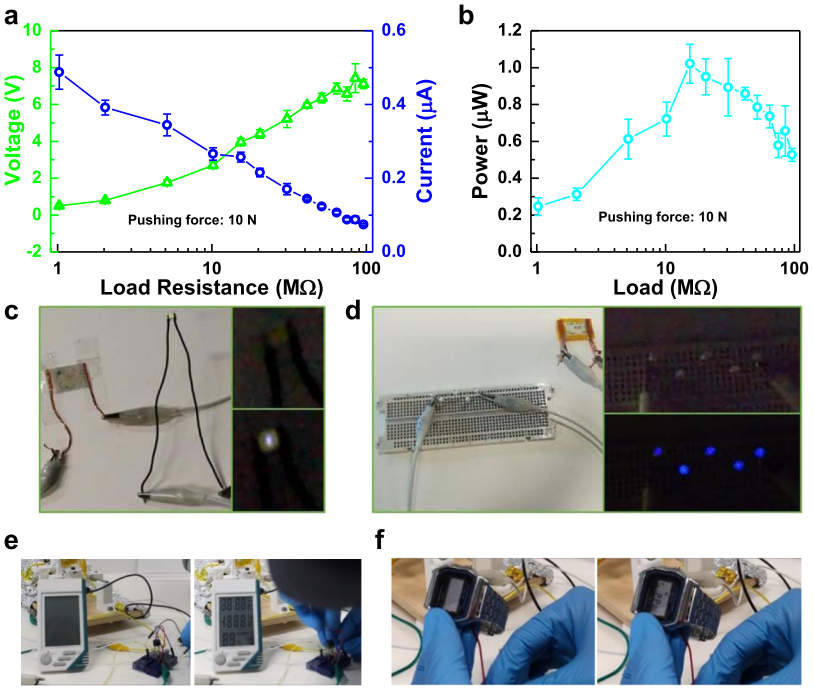

Figure 7. Output (a) voltage and current and (b) instantaneous power generated from the $ZnSnO_3$@PDMS microstructured films with the optimized configuration under several load resistances. Photographs of a device directly connected to (c) a single white LED and (d) five blue LEDs in series, with the respective insets showing the LED/LEDs off and on (driven by the energy of the nanogenerator). Photographs of (e) an electronic humidity sensor and (f) a digital watch being powered up by a 10 μF capacitor previously charged by the nanogenerator.

https://dx.doi.org/10.1021/acsami.9b21636
ACS Appl. Mater. Interfaces 2020, 12, 18421−18430

Table 1. Performance Comparison of $ZnSnO_3$ Nanostructure-based Piezo/Triboelectric Harvesters

material	stimulus/applied force	output voltage	output current	instantaneous power density	year/refs
single-$ZnSnO_3$ microbelt@high temperature process	compressive strain (0.33−1.20 Hz) N/A	110 mV	80 nA	N/A	2012/[26]
single-$ZnSnO_3$ microbelt@high temperature process	compressive strain (0.30−1.66 Hz) N/A	5.3 V	0.13 μA	11 $\mu W \cdot cm^{-3}$	2012/[59]
$ZnSnO_3$ nanocubes@PDMS	motion of vehicle tires N/A	20 V	1 $\mu A \cdot cm^{-2}$		2014/[33]
$ZnSnO_3$/MWCNTs	strain N/A	40 V	0.4 μA	10.8 $\mu W \cdot cm^{-3}$	2015/[32]
$ZnSnO_3$ nanocubes@PDMS	linear motor/bending (1.5−3 Hz) N/A	400 V	28 μA	280 $\mu W \cdot cm^{-2}$	2015/[35]
$ZnSnO_3$ nanocubes@PVDF	fatigue testing system (1−7 Hz) 489 N	520 V	2.7 $\mu A \cdot m^{-2}$		2016/[36]
$ZnSnO_3$ nanocubes@PVC	human finger (1−10 Hz) N/A	40 V	1.4 μA	≈3.7 $\mu W \cdot cm^{-2}$	2016/[37]
$ZnSnO_3$ nanoplates@PDMS	bending (2 Hz) N/A	20 V	0.6 μA		2017/[5]
$ZnSnO_3$ nanocubes@PDMS + TENG	hand stabbing mechanism N/A	50 V (PNG) 300 V (hybrid)		10.4 mW·cm^{-2} (hybrid)	2017/[60]
$ZnSnO_3$ nanocubes@PDMS	footstep N/A	18 V	8 mA		2019/[61]
$ZnSnO_3$ nanowires@PDMS	pen >100 N	≈120 V	≈13 μA	≈230 $\mu W \cdot cm^{-2}$	this work

does not seem to produce a significant influence. Table S2 presents the peak-to-peak output voltage and current values of all the devices shown in Figure 4a,b. The configuration with aligned microcones with a gap between cones <100 μm has the best performance with a peak-to-peak voltage of 8.7 V and a peak-to-peak current of 1.25 μA, possibly because the density of cones in this configuration is smaller than in the configurations with a gap between cones of 0 μm, and so the forces get more concentrated in the first configuration, leading to a greater deformation of the microcones. This effect has been shown by other groups in capacitive sensors.[57,58] Additionally, the microcones for a gap between cones <100 μm are higher than the microcones with a gap between cones of 0 μm because the latter ones suffer from a fusion effect as a consequence of their fabrication process (Figure S4, please check ref 45 for further details). Therefore, there is a greater volume to be compressed in the configuration with a gap between cones <100 μm, and so a greater number of nanowires may be bent, thus increasing their piezoelectric signal.

Pushing Force Dependence. To stimulate the device with the optimized configuration with larger forces, different levels of tapping force using a pen (contact area of 0.7 cm^2) were tested. Figure 5 shows the peak-to-peak voltage and current outputs obtained in these experiments. The results highlight that the nature of the stimuli applied by the home-made machine is different from these manual stimuli: while the first resembles a continuous stimulus, the latter are more impulse like. Therefore, for similar forces applied manually (between 12 and 15 N), the device has a higher voltage and current output with values of 31.2 V and 1.8 μA, corresponding to an instantaneous power density of 8.2 $\mu W \cdot cm^{-2}$. The maximum output of the device with this type of stimuli was ≈120 V and ≈13 μA, corresponding to an instantaneous power density of ≈230 $\mu W \cdot cm^{-2}$.

Device Stability. In order to study device stability over time, 12,000 cycles were performed for 100 min without interruption on a nanogenerator with the optimized $ZnSnO_3$@PDMS microstructured films. As shown in Figure 6a,b, despite a slight variation in the output, mostly at initial cycles because of the unoptimized assembly of the PET/ITO top contact with copper tape, the device presents a stable performance even after being pushed over 12,000 cycles. The microcones present no signs of degradation after this test, as shown in Figure S7. After one month of the initial measurements (Figure 4a,b), the same level of performance is observed, as presented in Figure S8.

Proof of Concept. To test the device for a practical application, it is relevant to investigate the electric power that the device can provide with a load. Therefore, the output voltage, current, and instantaneous power of the device with the optimized configuration were evaluated under several load resistances, as shown in Figure 7a,b. The output current decreases with an increasing load resistance while the output voltage increases. The instantaneous power increases with the load resistance, reaching a maximum peak of 1 μW with 15 MΩ, and then decreasing for higher load resistances.

The device with the optimized configuration was then directly connected to one white light-emitting diode (LED) or five blue LEDs in series. The $I-V$ curves of the single and five LEDs are shown in Figure S9 and highlight that the single white LED needs at least 2.3 V and 1.56 μA to light up, while the five blue LEDs in series need 11.4 V and 0.13 μA. Figure 7c,d shows that after manually pushing the device either the single white LED (Supporting Information Video S4) or the multiple blue LEDs in series (Supporting Information Video S5) could light up.

Powering of small electrical devices was also tested with the optimized nanogenerator. For this end, the nanogenerator was stimulated to charge a 10 μF capacitor through a full-wave rectifier over 10−15 min. The capacitor was then connected to an electronic humidity sensor, a digital watch, and a dial watch to successfully switch them on, as shown in Figure 7e,f and Supporting Information Video S6. The circuit schematic and the capacitor charging curve are presented in Figure S10.

Table 1 shows a comparison between the device with the best performance produced in this work with the literature related to the use of $ZnSnO_3$ nanostructures in piezo/triboelectric harvesters. Although a direct comparison is not possible because of the lack of some information from other works, the device produced herein shows a high performance for energy harvesting from stimuli with a moderate force, compatible with everyday activities. For example, the nanogenerator could be attached to the bottom of shoes to get energy from walking or running. The instantaneous power density reached herein is also one of the highest reported so far, and only the $ZnSnO_3$ nanocubes@PDMS composite reported by Wang et al.[35] has a higher response, but due to the lack of information and quantification about the applied force,

https://dx.doi.org/10.1021/acsami.9b21636
ACS Appl. Mater. Interfaces 2020, 12, 18421−18430

a direct comparison is not feasible. Nevertheless, these results highlight the potential for powering portable electronics. Furthermore, given the higher flexibility of the wire morphology when compared with cubes or other structures, the optimization of the weight ratio between $ZnSnO_3$ nanowires and PDMS is expected to result in devices with a greater output for the same stimulus, when compared to those presented in Table 1.

CONCLUSIONS

PENGs were fabricated using a composite film of PDMS and $ZnSnO_3$ nanowires produced by a hydrothermal synthesis at only 200 °C. The $ZnSnO_3$ nanowires clearly showed piezoelectric properties through PFM measurements, reaching a d_{33} of 23 ± 4 pm/V, considerably larger than the d_{33} recorded for ZnO nanowires. Several microstructuration designs for the composite films were also studied to enhance the performance of the nanogenerators. The microcones helped to improve the piezoelectric signal coming from the nanowires through an increased efficiency in the force transmission. Such an effect results in a better performance achieved for the configuration with aligned microcones with a gap between cones <100 μm, showing a peak-to-peak voltage around 8.7 V and a peak-to-peak current of 1.25 μA (instantaneous power density of 3.24 $\mu W \cdot cm^{-2}$) for a 10 N stimulus applied by a home-made machine. When stimulated manually with a pen (a force over 100 N), a maximum output of 120 V and 13 μA was achieved, with an estimated instantaneous power density of 230 $\mu W \cdot cm^{-2}$. This instantaneous power density is enough for practical applications, such as lighting up LEDs and charging capacitors to levels enabling powering up small electronic devices, showing great potential for energy harvesting in wearables.

ASSOCIATED CONTENT

Supporting Information

The Supporting Information is available free of charge at https://pubs.acs.org/doi/10.1021/acsami.9b21636.

Photograph of the home-made machine used for the pushing tests; synthesis of ZnO nanowires; morphological and structural characterization of ZnO nanowires; piezoelectric coefficient of some of 1D piezoelectric nanostructures produced by the hydrothermal synthesis; electrostatic force microscopy of $ZnSnO_3$ and ZnO nanowires on the ITO substrate; SEM images; output voltage and current of devices with only PDMS films; peak-to-peak voltage and current output values from the $ZnSnO_3$@PDMS devices with different architectures (shown in Figure 4b,c); representative schematic of the charge generation and displacement mechanism for both the piezoelectric and triboelectric effects in microstructured devices; the output voltage and current generated from the $ZnSnO_3$@PDMS microstructured films; $I-V$ characteristic curves; and circuit schematic (PDF)

Video of home-made machine used in the measurements (MP4)

Video of a microstructured nanogenerator being compressed (AVI)

Video of an unstructured nanogenerator being compressed (AVI)

Video of a single LED being lit-up by microstructured nanogenerator (AVI)

Video of multiple LEDs being lit-up by microstructured nanogenerator (AVI)

Video of several electronic devices being turned on by connecting them to a 10 μF capacitor (MP4))

AUTHOR INFORMATION

Corresponding Authors

Rui Igreja − *i3N/CENIMAT, Department of Materials Science, Faculty of Science and Technology, Universidade NOVA de Lisboa and CEMOP/UNINOVA, 2829-516 Caparica, Portugal*; Email: rni@fct.unl.pt

Pedro Barquinha − *i3N/CENIMAT, Department of Materials Science, Faculty of Science and Technology, Universidade NOVA de Lisboa and CEMOP/UNINOVA, 2829-516 Caparica, Portugal*; orcid.org/0000-0002-5446-2759; Email: pmcb@fct.unl.pt

Authors

Ana Rovisco − *i3N/CENIMAT, Department of Materials Science, Faculty of Science and Technology, Universidade NOVA de Lisboa and CEMOP/UNINOVA, 2829-516 Caparica, Portugal*; orcid.org/0000-0001-6240-3743

Andreia dos Santos − *i3N/CENIMAT, Department of Materials Science, Faculty of Science and Technology, Universidade NOVA de Lisboa and CEMOP/UNINOVA, 2829-516 Caparica, Portugal*

Tobias Cramer − *Department of Physics and Astronomy, University of Bologna, 40127 Bologna, Italy*

Jorge Martins − *i3N/CENIMAT, Department of Materials Science, Faculty of Science and Technology, Universidade NOVA de Lisboa and CEMOP/UNINOVA, 2829-516 Caparica, Portugal*

Rita Branquinho − *i3N/CENIMAT, Department of Materials Science, Faculty of Science and Technology, Universidade NOVA de Lisboa and CEMOP/UNINOVA, 2829-516 Caparica, Portugal*; orcid.org/0000-0001-9771-8366

Hugo Águas − *i3N/CENIMAT, Department of Materials Science, Faculty of Science and Technology, Universidade NOVA de Lisboa and CEMOP/UNINOVA, 2829-516 Caparica, Portugal*

Beatrice Fraboni − *Department of Physics and Astronomy, University of Bologna, 40127 Bologna, Italy*

Elvira Fortunato − *i3N/CENIMAT, Department of Materials Science, Faculty of Science and Technology, Universidade NOVA de Lisboa and CEMOP/UNINOVA, 2829-516 Caparica, Portugal*

Rodrigo Martins − *i3N/CENIMAT, Department of Materials Science, Faculty of Science and Technology, Universidade NOVA de Lisboa and CEMOP/UNINOVA, 2829-516 Caparica, Portugal*

Complete contact information is available at: https://pubs.acs.org/10.1021/acsami.9b21636

Author Contributions

A.R. and A.d.S. contributed equally. The manuscript was written through contributions of all authors. All the authors have given approval to the final version of the manuscript.

Funding

This work is funded by FEDER funds through the COMPETE 2020 Programme and National Funds through FCT—

Portuguese Foundation for Science and Technology under the project number POCI-01-0145-FEDER-007688, Reference UID/CTM/50025 and the doctoral grants research numbers SFRH/BD/131836/2017 and SFRH/BD/122286/2016. A.d.S. acknowledges the support from the Portuguese Foundation for Science and Technology and MIT- Portugal through the scholarship PD/BD/105876/2014. This work also received funding from the European Community's H2020 program under grant agreement no. 716510 (ERC-2016-STG TREND) and no. 685758 (1D-Neon).

Notes

The authors declare no competing financial interest.

REFERENCES

(1) Lee, K. Y.; Gupta, M. K.; Kim, S.-W. Transparent Flexible Stretchable Piezoelectric and Triboelectric Nanogenerators for Powering Portable Electronics. *Nano Energy* **2015**, *14*, 139−160.

(2) Chen, J.; Wang, Z. L. Reviving Vibration Energy Harvesting and Self-Powered Sensing by a Triboelectric Nanogenerator. *Joule* **2017**, *1*, 480−521.

(3) Quan, T.; Yang, Y. Fully Enclosed Hybrid Electromagnetic−Triboelectric Nanogenerator to Scavenge Vibrational Energy. *Nano Res.* **2016**, *9*, 2226−2233.

(4) Rahimi, A.; Zorlu, Öo.; Muhtaroğlu, A.; Külah, H. A Compact Electromagnetic Vibration Harvesting System with High Performance Interface Electronics. *Procedia Eng.* **2011**, *25*, 215−218.

(5) Guo, R.; Guo, Y.; Duan, H.; Li, H.; Liu, H. Synthesis of Orthorhombic Perovskite-Type ZnSnO3 Single-Crystal Nanoplates and Their Application in Energy Harvesting. *ACS Appl. Mater. Interfaces* **2017**, *9*, 8271−8279.

(6) Li, W.; Torres, D.; Díaz, R.; Wang, Z.; Wu, C.; Wang, C.; Lin Wang, Z.; Sepúlveda, N. Nanogenerator-Based Dual-Functional and Self-Powered Thin Patch Loudspeaker or Microphone for Flexible Electronics. *Nat. Commun.* **2017**, *8*, 15310.

(7) Chen, B.; Yang, Y.; Wang, Z. L. Scavenging Wind Energy by Triboelectric Nanogenerators. *Adv. Energy Mater.* **2018**, *8*, 1702649.

(8) Chen, X.; Li, X.; Shao, J.; An, N.; Tian, H.; Wang, C.; Han, T.; Wang, L.; Lu, B. High-Performance Piezoelectric Nanogenerators with Imprinted P(VDF-TrFE)/BaTiO3 Nanocomposite Micropillars for Self-Powered Flexible Sensors. *Small* **2017**, *13*, 1−12.

(9) Askari, H.; Khajepour, A.; Khamesee, M. B.; Saadatnia, Z.; Wang, Z. L. Piezoelectric and Triboelectric Nanogenerators: Trends and Impacts. *Nano Today* **2018**, *22*, 10−13.

(10) Wu, Y.; Zhong, X.; Wang, X.; Yang, Y.; Wang, Z. L. Hybrid Energy Cell for Simultaneously Harvesting Wind, Solar, and Chemical Energies. *Nano Res.* **2014**, *7*, 1631−1639.

(11) Yang, Y.; Wang, Z. L. Hybrid Energy Cells for Simultaneously Harvesting Multi-Types of Energies. *Nano Energy* **2015**, *14*, 245−256.

(12) Wang, X.; Yang, B.; Liu, J.; Zhu, Y.; Yang, C.; He, Q. A Flexible Triboelectric-Piezoelectric Hybrid Nanogenerator Based on P(VDF-TrFE) Nanofibers and PDMS/MWCNT for Wearable Devices. *Sci. Rep.* **2016**, *6*, 1−10.

(13) Ye, S.; Cheng, C.; Chen, X.; Chen, X.; Shao, J.; Zhang, J.; Hu, H.; Tian, H.; Li, X.; Ma, L.; Jia, W. High-Performance Piezoelectric Nanogenerator Based on Microstructured P(VDF-TrFE)/BNNTs Composite for Energy Harvesting and Radiation Protection in Space. *Nano Energy* **2019**, *60*, 701−714.

(14) Zhang, L.; Gui, J.; Wu, Z.; Li, R.; Wang, Y.; Gong, Z.; Zhao, X.; Sun, C.; Guo, S. Enhanced Performance of Piezoelectric Nanogenerator Based on Aligned Nanofibers and Three-Dimensional Interdigital Electrodes. *Nano Energy* **2019**, *65*, 103924.

(15) Wang, Z. L. Piezoelectric Nanogenerators Based on Zinc Oxide Nanowire Arrays. *Science* **2006**, *312*, 242−246.

(16) Zhao, Y.; Lai, X.; Deng, P.; Nie, Y.; Zhang, Y.; Xing, L.; Xue, X. Pt/ZnO Nanoarray Nanogenerator as Self-Powered Active Gas Sensor with Linear Ethanol Sensing at Room Temperature. *Nanotechnology* **2014**, *25*, 115502.

(17) Zhao, Y.; Deng, P.; Nie, Y.; Wang, P.; Zhang, Y.; Xing, L.; Xue, X. Biomolecule-Adsorption-Dependent Piezoelectric Output of ZnO Nanowire Nanogenerator and Its Application as Self-Powered Active Biosensor. *Biosens. Bioelectron.* **2014**, *57*, 269−275.

(18) Pimentel, A.; Nunes, D.; Duarte, P.; Rodrigues, J.; Costa, F. M.; Monteiro, T.; Martins, R.; Fortunato, E. Synthesis of Long ZnO Nanorods under Microwave Irradiation or Conventional Heating. *J. Phys. Chem. C* **2014**, *118*, 14629−14639.

(19) Fortunato, E.; Gonçalves, A.; Pimentel, A.; Barquinha, P.; Gonçalves, G.; Pereira, L.; Ferreira, I.; Martins, R. Zinc Oxide, a Multifunctional Material: From Material to Device Applications. *Appl. Phys. Mater. Sci. Process* **2009**, *96*, 197−205.

(20) Inaguma, Y.; Yoshida, M.; Katsumata, T. A Polar Oxide ZnSnO3 with a LiNbO3-Type Structure. *J. Am. Chem. Soc.* **2008**, *130*, 6704−6705.

(21) Sun, S.; Liang, S. Morphological Zinc Stannate: Synthesis, Fundamental Properties and Applications. *J. Mater. Chem. A* **2017**, *5*, 20534−20560.

(22) Baruah, S.; Dutta, J. Zinc Stannate Nanostructures: Hydrothermal Synthesis. *Sci. Technol. Adv. Mater.* **2011**, *12*, 013004.

(23) Gou, H.; Zhang, J.; Li, Z.; Wang, G.; Gao, F.; Ewing, R. C.; Lian, J. Energetic Stability, Structural Transition, and Thermodynamic Properties of ZnSnO3. *Appl. Phys. Lett.* **2011**, *98*, 091914.

(24) Rovisco, A.; Branquinho, R.; Martins, J.; Oliveira, M. J.; Nunes, D.; Fortunato, E.; Martins, R.; Barquinha, P. Seed-Layer Free Zinc Tin Oxide Tailored Nanostructures for Nanoelectronic Applications: Effect of Chemical Parameters. *ACS Appl. Nano Mater.* **2018**, *1*, 3986−3997.

(25) Bora, T.; Al-Hinai, M. H.; Al-Hinai, A. T.; Dutta, J. Phase Transformation of Metastable ZnSnO3 Upon Thermal Decomposition by In-Situ Temperature-Dependent Raman Spectroscopy. *J. Am. Ceram. Soc.* **2015**, *98*, 4044−4049.

(26) Wu, J. M.; Xu, C.; Zhang, Y.; Wang, Z. L. Lead-Free Nanogenerator Made from Single ZnSnO3 Microbelt. *ACS Nano* **2012**, *6*, 4335−4340.

(27) Fu, Y.; Nie, Y.; Zhao, Y.; Wang, P.; Xing, L.; Zhang, Y.; Xue, X. Detecting Liquefied Petroleum Gas (LPG) at Room Temperature Using ZnSnO3/ZnO Nanowire Piezo-Nanogenerator as Self-Powered Gas Sensor. *ACS Appl. Mater. Interfaces* **2015**, *7*, 10482−10490.

(28) Wu, J. M.; Xu, C.; Zhang, Y.; Yang, Y.; Zhou, Y.; Wang, Z. L. Flexible and Transparent Nanogenerators Based on a Composite of Lead-Free ZnSnO3 Triangular-Belts. *Adv. Mater.* **2012**, *24*, 6094−6099.

(29) Wu, J. M.; Chen, C.-Y.; Zhang, Y.; Chen, K.-H.; Yang, Y.; Hu, Y.; He, J.-H.; Wang, Z. L. Ultrahigh Sensitive Piezotronic Strain Sensors Based on a ZnSnO3 Nanowire/Microwire. *ACS Nano* **2012**, *6*, 4369−4374.

(30) Choi, K. H.; Siddiqui, G. U.; Yang, B.-s.; Mustafa, M. Synthesis of ZnSnO3 Nanocubes and Thin Film Fabrication of (ZnSnO3/PMMA) Composite through Electrospray Deposition. *J. Mater. Sci. Mater. Electron.* **2015**, *26*, 5690−5696.

(31) Yang, Y. J.; Aziz, S.; Mehdi, S. M.; Sajid, M.; Jagadeesan, S.; Choi, K. H. Highly Sensitive Flexible Human Motion Sensor Based on ZnSnO3/PVDF Composite. *J. Electron. Mater.* **2017**, *46*, 4172−4179.

(32) Alam, M. M.; Ghosh, S. K.; Sultana, A.; Mandal, D. Lead-Free ZnSnO3/MWCNTs-Based Self-Poled Flexible Hybrid Nanogenerator for Piezoelectric Power Generation. *Nanotechnology* **2015**, *26*, 165403.

(33) Lee, K. Y.; Kim, D.; Lee, J.-H.; Kim, T. Y.; Gupta, M. K.; Kim, S.-W. Unidirectional High-Power Generation via Stress-Induced Dipole Alignment from ZnSnO3 Nanocubes/Polymer Hybrid Piezoelectric Nanogenerator. *Adv. Funct. Mater.* **2014**, *24*, 37−43.

(34) Wu, J. M.; Chen, K.-H.; Zhang, Y.; Wang, Z. L. A Self-Powered Piezotronic Strain Sensor Based on Single ZnSnO3 Microbelts. *RSC Adv.* **2013**, *3*, 25184.

(35) Wang, G.; Xi, Y.; Xuan, H.; Liu, R.; Chen, X.; Cheng, L. Hybrid Nanogenerators Based on Triboelectrification of a Dielectric Composite Made of Lead-Free ZnSnO3 Nanocubes. *Nano Energy* **2015**, *18*, 28−36.

https://dx.doi.org/10.1021/acsami.9b21636
ACS Appl. Mater. Interfaces 2020, 12, 18421−18430

(36) Soin, N.; Zhao, P.; Prashanthi, K.; Chen, J.; Ding, P.; Zhou, E.; Shah, T.; Ray, S. C.; Tsonos, C.; Thundat, T.; Siores, E.; Luo, J. High Performance Triboelectric Nanogenerators Based on Phase-Inversion Piezoelectric Membranes of Poly(Vinylidene Fluoride)-Zinc Stannate (PVDF-ZnSnO3) and Polyamide-6 (PA6). *Nano Energy* **2016**, *30*, 470−480.
(37) Paria, S.; Karan, S. K.; Bera, R.; Das, A. K.; Maitra, A.; Khatua, B. B. A Facile Approach to Develop a Highly Stretchable PVC/ZnSnO3 Piezoelectric Nanogenerator with High Output Power Generation for Powering Portable Electronic Devices. *Ind. Eng. Chem. Res.* **2016**, *55*, 10671−10680.
(38) Yang, Y.; Zhang, H.; Lin, Z.-H.; Zhou, Y. S.; Jing, Q.; Su, Y.; Yang, J.; Chen, J.; Hu, C.; Wang, Z. L. Human Skin Based Triboelectric Nanogenerators for Harvesting Biomechanical Energy and as Self-Powered Active Tactile Sensor System. *ACS Nano* **2013**, *7*, 9213−9222.
(39) Lee, S.; Lee, Y.; Kim, D.; Yang, Y.; Lin, L.; Lin, Z.-H.; Hwang, W.; Wang, Z. L. Triboelectric Nanogenerator for Harvesting Pendulum Oscillation Energy. *Nano Energy* **2013**, *2*, 1113−1120.
(40) Seol, M.-L.; Woo, J.-H.; Lee, D.-I.; Im, H.; Hur, J.; Choi, Y.-K. Nature-Replicated Nano-in-Micro Structures for Triboelectric Energy Harvesting. *Small* **2014**, *10*, 3887−3894.
(41) Wang, X.; Han, X.; Dong, L.; Zhang, H.; Pan, C.; Zhai, J.; Wang, Z. L.; Du, W. Self-Powered High-Resolution and Pressure-Sensitive Triboelectric Sensor Matrix for Real-Time Tactile Mapping. *Adv. Mater.* **2016**, *28*, 2896−2903.
(42) Lin, L.; Xie, Y.; Wang, S.; Niu, S.; Wen, X.; Wang, Z. L.; Wu, W. Triboelectric Active Sensor Array for Self-Powered Static and Dynamic Pressure Detection and Tactile Imaging. *ACS Nano* **2013**, *7*, 8266−8274.
(43) Fan, F.-R.; Lin, L.; Zhu, G.; Wu, W.; Zhang, R.; Wang, Z. L. Transparent Triboelectric Nanogenerators and Self-Powered Pressure Sensors Based on Micropatterned Plastic Films. *Nano Lett.* **2012**, *12*, 3109−3114.
(44) Zhu, Y.; Yang, B.; Liu, J.; Wang, X.; Wang, L.; Chen, X.; Yang, C. A Flexible and Biocompatible Triboelectric Nanogenerator with Tunable Internal Resistance for Powering Wearable Devices. *Sci. Rep.* **2016**, *6*, 22233.
(45) dos Santos, A.; Pinela, N.; Alves, P.; Santos, R.; Fortunato, E.; Martins, R.; Águas, H.; Igreja, R. Piezoresistive E-Skin Sensors Produced with Laser Engraved Molds. *Adv. Electron. Mater.* **2018**, *4*, 1800182−1800192.
(46) dos Santos, A.; Pinela, N.; Alves, P.; Santos, R.; Fortunato, E.; Martins, R.; Águas, H.; Igreja, R. E-Skin Pressure Sensors Made by Laser Engraved PDMS Molds. *Proceedings* **2018**, *2*, 1039.
(47) dos Santos, A.; Pinela, N.; Alves, P.; Santos, R.; Farinha, R.; Fortunato, E.; Martins, R.; Águas, H.; Igreja, R. E-Skin Bimodal Sensors for Robotics and Prosthesis Using PDMS Molds Engraved by Laser. *Sensors* **2019**, *19*, 899.
(48) Rovisco, A.; Branquinho, R.; Martins, J.; Fortunato, E.; Martins, R.; Barquinha, P. Growth Mechanism of Seed-Layer Free ZnSnO3 Nanowires: Effect of Physical Parameters. *Nanomaterials* **2019**, *9*, 1002.
(49) Samouco, A.; Marques, A. C.; Pimentel, A.; Martins, R.; Fortunato, E. Laser-Induced Electrodes towards Low-Cost Flexible UV ZnO Sensors. *Flexible Printed Electron.* **2018**, *3*, 044002.
(50) Biswas, A.; Saha, S.; Jana, N. R. ZnSnO 3 Nanoparticle-Based Piezocatalysts for Ultrasound-Assisted Degradation of Organic Pollutants. *ACS Appl. Nano Mater.* **2019**, *2*, 1120−1128.
(51) Xue, X. Y.; Chen, Y. J.; Wang, Y. G.; Wang, T. H. Synthesis and Ethanol Sensing Properties of ZnSnO3 Nanowires. *Appl. Phys. Lett.* **2005**, *86*, 233101.
(52) Placke, A.; Kumar, A.; Priya, S. Synthesis and Behavior of Cetyltrimethyl Ammonium Bromide Stabilized Zn1+xSnO3+x ($0 \leq x \leq 1$) Nano-Crystallites. *PLoS One* **2016**, *11*, No. e0156246.
(53) Fu, Y.; Nie, Y.; Zhao, Y.; Wang, P.; Xing, L.; Zhang, Y.; Xue, X. Detecting Liquefied Petroleum Gas (LPG) at Room Temperature Using ZnSnO3ZnO Nanowire Piezo-Nanogenerator as Self-Powered Gas Sensor. *ACS Appl. Mater. Interfaces* **2015**, *7*, 10482−10490.
(54) Broitman, E.; Soomro, M. Y.; Lu, J.; Willander, M.; Hultman, L. Nanoscale Piezoelectric Response of ZnO Nanowires Measured Using a Nanoindentation Technique. *Phys. Chem. Chem. Phys.* **2013**, *15*, 11113−11118.
(55) Ghasemian, M. B.; Lin, Q.; Adabifiroozjaei, E.; Wang, F.; Chu, D.; Wang, D. Morphology Control and Large Piezoresponse of Hydrothermally Synthesized Lead-Free Piezoelectric (Bi0.5Na0.5)-TiO3 Nanofibres. *RSC Adv.* **2017**, *7*, 15020−15026.
(56) Moheimani, S. O. R.; Fleming, A. J. *Piezoelectric Transducers for Vibration Control and Damping*; Springer, 2006.
(57) Schwartz, G.; Tee, B. C.-K.; Mei, J.; Appleton, A. L.; Kim, D. H.; Wang, H.; Bao, Z. Flexible Polymer Transistors with High Pressure Sensitivity for Application in Electronic Skin and Health Monitoring. *Nat. Commun.* **2013**, *4*, 1859−1867.
(58) Ji, Z.; Zhu, H.; Liu, H.; Liu, N.; Chen, T.; Yang, Z.; Sun, L. The Design and Characterization of a Flexible Tactile Sensing Array for Robot Skin. *Sensors* **2016**, *16*, 2001.
(59) Wu, J. M.; Xu, C.; Zhang, Y.; Yang, Y.; Zhou, Y.; Wang, Z. L. Flexible and Transparent Nanogenerators Based on a Composite of Lead-Free ZnSnO3 Triangular-Belts. *Adv. Mater.* **2012**, *24*, 6094−6099.
(60) Hassan, G.; Khan, F.; Hassan, A.; Ali, S.; Bae, J.; Lee, C. H. A Flat-Panel-Shaped Hybrid Piezo/Triboelectric Nanogenerator for Ambient Energy Harvesting. *Nanotechnology* **2017**, *28*, 175402.
(61) Ali, S.; Khan, S.; Bermak, A. All-Printed Human Activity Monitoring and Energy Harvesting Device for Internet of Thing Applications. *Sensors* **2019**, *19*, 1197.

https://dx.doi.org/10.1021/acsami.9b21636
ACS Appl. Mater. Interfaces 2020, 12, 18421−18430